scientific reports

Check for updates

OPEN

Fabrication of nanoscale T-shaped reentrant structures and its hydrophobic analysis

Zeping Li[1,2], Qing Wan[1,2], Jiaqi Wang[3] & Geng Wang[1,2]✉

The present work proposes a facile method for fabricating robust hydrophobic surfaces with T-shaped reentrant nanostructures based on nano-patterning approach. The prepared surface demonstrates regularly arrangement over a large area. The hydrophobic stability of the prepared surface was analyzed theoretically using the Gibbs free energy approach, followed by being investigated experimentally. Experimental results show that the T-shaped reentrant nanostructures can significantly improve the hydrophobic stability of the surface, which is in line with the theoretical predictions. The proposed preparation method for T-shaped reentrant nanostructures provides a cost-effective and convenient way to fabricate robust hydrophobic surfaces.

Surface hydrophobicity, featuring high contact angles and low contact angle hysteresis, has numerous attractive practical applications such as antifouling[1–4], self-cleaning[5], windshield[6], anti-fogging[7,8], anti-icing[9], and microfluidic control[10–13]. One method of maintaining hydrophobicity is to develop low surface tension coatings to ensure that the Cassie–Baxter (non-wetting) state remains in the minimum free energy state, but the coating is prone to surface contamination and degradation. To improve hydrophobic stability, reentrant or negative-slope structures followed by modification with fluorinated materials are developed to obtain upward net forces for lifting a droplet, even for low surface-tension liquids[14]. T-shaped reentrant structures exhibit the highest performance in liquid repellency concerning pressure balance, pinning effects, and surface curvature conditions[14]. Nanostructured reentrant surfaces represent practical advantages on the unique optical properties[15,16], excellent pressure robustness[17,18], modulating immune response[19], controlling bacterial adhesion[20], and biofilm formation[21,22], compared with microscale structures. However, their preparation can be challenging, complicated, and costly. Despite random growth of the nanostructured surfaces is more straightforward and cost-effective, the fabricated irregular surfaces encounter less effective hydrophobicity[14]. T-shaped reentrant nanostructures have a significant influence on the wetting properties of solid surfaces.

In this report, we present a facile method for fabricating T-shaped reentrant nanostructures on mechanically stable silicon wafer based on selective etching with nano-patterning approach. The hydrophobicity robustness of the prepared T-shaped reentrant nanostructures is evaluated theoretically using the Gibbs free energy approach, followed by being investigated experimentally. Experimental results show that, the T-shaped reentrant nanostructures can significantly improve the hydrophobic stability of the surface, which is in line with our theoretical predictions.

Results and discussion

Surface morphology

The SEM images in Fig. 1a exhibit a highly ordered Cr nanoparticle array with a thickness of ~ 100 nm, and an intentionally retained residual AAO mask for comparison. The Cr nanoparticles were successfully and regularly deposited on the Si surface through through-hole AAO evaporation mask. Subsequently, the Si substrate was subjected to XeF_2 isotropic etching using Cr nanoparticles as a mask to prepare T-shaped reentrant nanostructures with high aspect ratios, as shown in Fig. 1b. The SEM images in Fig. 1c display large-scale, regularly arranged T-shaped reentrant nanostructures. The geometric parameters of fabricated T-shaped reentrant nanostructures are shown in Table 1. Based on the tunable characteristics of AAO mask with tunable pore diameter and cell size and its non-lithographic properties[23], the presented nano-patterning approach will offer attractive advantages, such as large pattern area, high throughput, low cost.

[1]School of Electronic and Information Engineering, Hubei University of Science and Technology, Xianning 437100, People's Republic of China. [2]Key Laboratory of Photoelectric Sensing and Intelligent Control, Hubei University of Science and Technology, Xianning 437100, Hubei, People's Republic of China. [3]School of Foreign Languages, Wuhan Institute of Technology, Wuhan 430205, Hubei, People's Republic of China. ✉email: 42912868@qq.com

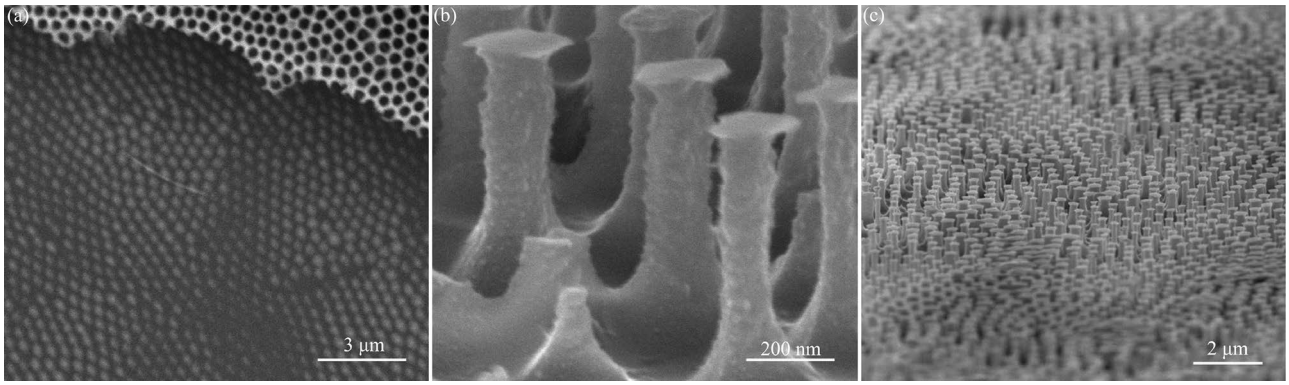

Figure 1. The SEM images of (**a**) Cr nanoparticles and partially unremoved AAO mask, (**b**) T-shaped reentrant nanostructures, (**c**) large-area T-shaped reentrant nanostructures.

D (nm)	d (nm)	H (nm)	h (nm)	P (nm)	$r = r_f$ (x = H)
200	140	600	20	500	1.98

Table 1. The geometric parameters of fabricated T-shaped reentrant nanostructures. Herein r represents the roughness ratio of T-shaped reentrant nanostructures.

Theoretical analysis of the hydrophobic robustness. In our calculations, we assume various values for the temporary apparent contact angle ($0° < \theta_{app} < 180°$) at a specified distance (x/H) of the liquid–air interface from the surface of T-shaped cap (normalized with respect to the height of T-shaped reentrant nanostructures H). Then the areal Gibbs free energy density (G*) of the liquid drop is calculated for each θ_{app} and x/H. In order to facilitate easier visualization of the variation in the areal Gibbs free energy density of the T-shaped reentrant nanostructured surface, an uneven scale distribution of x-axis (x/H) was adopted in Fig. 2, which is based on the height of T-shaped cap (h = 20 nm) and the height of T-shaped pillar (H–h = 580 nm).

In Fig. 2a,b, a metastable composite interface corresponding to a global minimum in free energy is observed at x ~ 0, while a fully-wetted interface corresponding to a local minimum in free energy is observed at x ~ 600 nm. The liquid droplets keep in a metastable state with relatively low energy from x ~ 0 to x ~ 20 nm. There is a potential barrier at x ~ 20 nm as shown in Fig. 2c, and the liquid droplets from x ~ 0 to x ~ 20 nm would break through the barrier after being subjected to external pressure and reach x ~ 600 nm, which is a fully-wetted interface corresponding to a local minimum in free energy.

In Fig. 2d,e, a fully-wetted interface corresponding to a global minimum in free energy is observed at x ~ 600 nm, while a metastable composite interface corresponding to a local minimum in free energy is observed at x ~ 0. The liquid droplets keep in a metastable state with relatively low energy from x ~ 0 to x ~ 20 nm. There is a potential barrier at x ~ 20 nm as shown in Fig. 2f, and the liquid droplets from x ~ 0 to x ~ 20 nm would break through the barrier after being subjected to external pressure and reach x ~ 600 nm, which is a fully-wetted interface corresponding to a global minimum in free energy.

Surface wettability of T-shaped reentrant nanostructures

To evaluate the wetting properties, we selected five probing liquids with different surface tensions: hexadecane, toluene, olive oil, ethylene glycol, and DI water (see Table 2). The initial examination was conducted on a flat silicon surface coated with PFOTS (as depicted in Fig. 3). The measured θ_{app} decreased with increasing liquid surface tension. Our observations showed that the apparent contact angle (θ_{app}) decreased with a decrease in liquid surface tension while the transition from wetting to non-wetting ($\theta_{app} \approx 90°$) occurred at a critical surface tension (γ_C) of approximately 48.2 mN/m. Furthermore, the contact angle hysteresis (θ_{CAH}) remained around 20°. As expected, liquids with lower surface tensions exhibited wetting behavior on the smooth PFOTS/Si surface. In contrast, the wetting properties of the T-shaped reentrant nanostructured PFOTS/Si surface were also examined, and the results demonstrated that the surface displayed high contact angles and low contact angle hysteresis (less than 10°) for droplets of varying surface tensions. The inset shows optical image of DI water (transparent), olive oil (light yellow) and ethylene glycol (red) droplets on the T-shaped reentrant nanostructured PFOTS/Si surface. Notably, the T-shaped reentrant nanostructured surface exhibited structural colors when exposed to light.

Under dynamic impact conditions, the enhanced stability in withstanding the wetting transition has also been noted on the T-shaped reentrant PFOTS/Si surface. A high-speed digital camera was utilized to capture

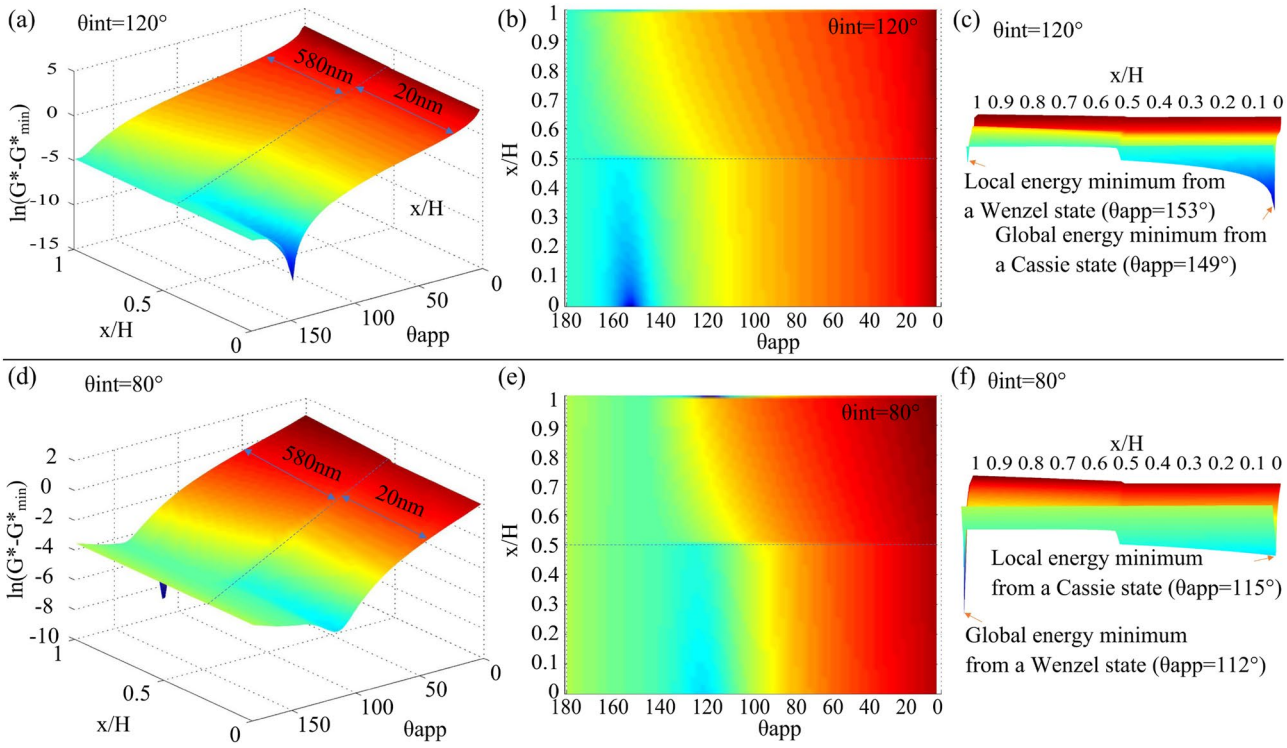

Figure 2. The change in the areal Gibbs free energy density. (**a**) The variation in the areal Gibbs free energy density for water propagating on a hydrophobic ($\theta_{int}=120°$) T-shaped reentrant nanostructured surface. (**b**) Top view of the energy diagram shown in (**a**). (**c**) Cross section view shown in (**a**). (**d**) The variation in the areal Gibbs free energy density for hexadecane propagating on an oleophilic ($\theta_{int}=80°$) T-shaped reentrant nanostructured surface. (**e**) Top view of the energy diagram shown in (**d**). (**f**) Cross section view shown in (**d**).

Liquid	Hexadecane	Toluene	Olive oil	Ethylene glycol	DI water
γ (mN/m)	27.5	28.3	29.8	48.2	72.6

Table 2. The surface tension of tested liquids measured on the flat and T-shaped reentrant PFOTS/Si surface.

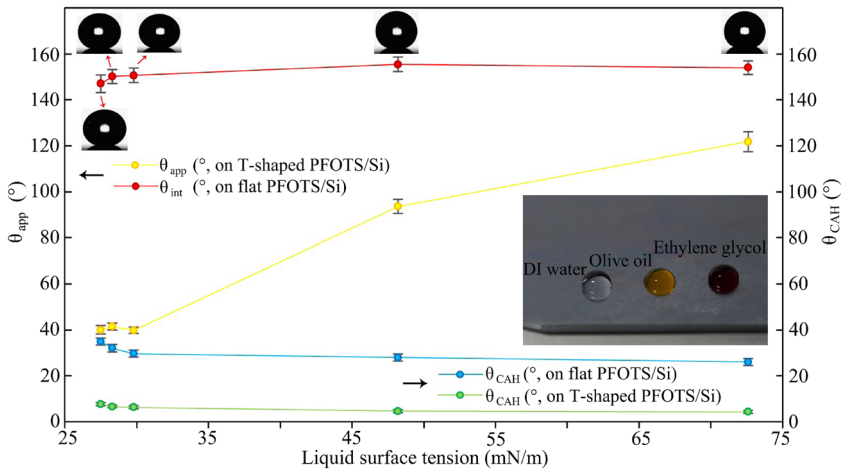

Figure 3. Wetting properties of the different liquids on the flat and T-shaped reentrant PFOTS/Si surface. The inset is optical image of DI water (transparent), olive oil (light yellow) and ethylene glycol (red) droplets on the T-shaped reentrant nanostructured PFOTS/Si surface.

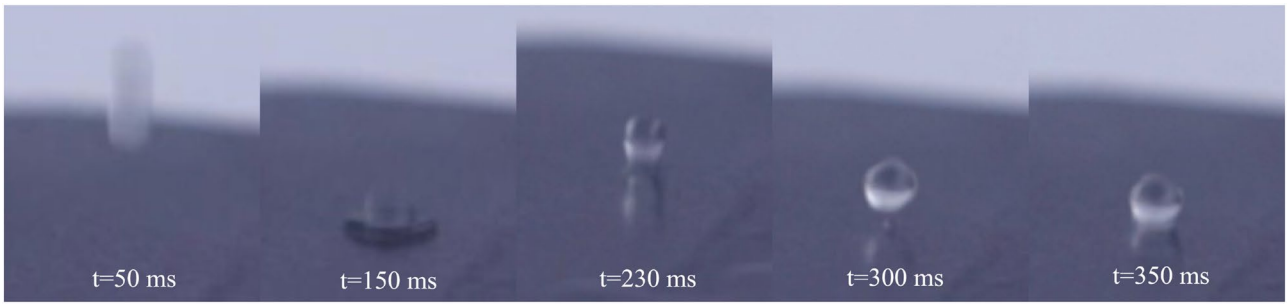

Figure 4. The surface of T-shaped reentrant nanostructured PFOTS/Si surface displayed the bouncing of hexadecane droplets as captured by a sequence of high-speed digital camera photograph.

a sequence of photos, and Fig. 4 illustrates the bouncing of ethylene glycol droplets on the T-shaped reentrant PFOTS/Si surface. Following release of the ethylene glycol droplets, they immediately contacted with PFOTS/Si's surface and spread out there. The droplet then contracted, fully rebounded, and detached from the PFOTS/Si surface before stabilizing there (Fig. 4, Supplemental Material, Movie 1).

Conclusions

In summary, we proposed a facile method to fabricate robust hydrophobic surfaces with T-shaped reentrant nanostructures. The prepared T-shaped reentrant nanostructures with regularly arrangement in a large area were demonstrated and the hydrophobic stability of the prepared surface was analyzed theoretically using the Gibbs free energy approach and experimentally. Experimental results show that the T-shaped reentrant nanostructures can significantly improve the hydrophobic stability of the surface, which is in line with the theoretical predictions. The proposed preparation method for T-shaped reentrant nanostructures provides a cost-effective and convenient way to fabricate robust hydrophobic surfaces.

Methods

Fabrication of T-shaped reentrant nanostructures

The through-hole anodic aluminium oxide (AAO) membranes were prepared by the well-known two-step anodization process (Fig. 5a) as our previous work[24]. The first anodization was carried out in 1% phosphoric acid and 0.01 M aluminum oxalate hydrate for 4 h at the temperature of 1 °C and voltage of 195 V. Perform a second anodization for 2.5 h under the same conditions. Subsequently, the pore-widening and pore-opening process was finished in 5% phosphoric acid solution for 50 min at 50 °C. The prepared AAO membranes were transferred onto the Si substrates in De-ionized (DI) water for keeping the membranes from twisting, folding and cracking (Fig. 5b). To achieve good mechanical robustness, a silicon wafer with the high Young's modulus

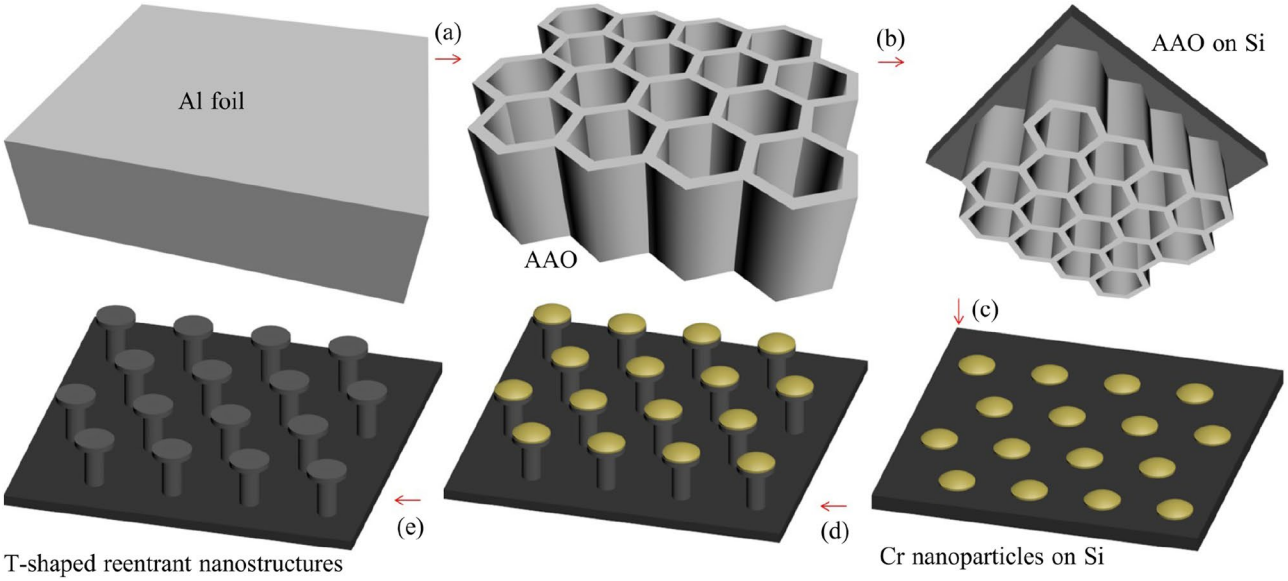

Figure 5. Schematic diagram of the fabrication process for T-shaped reentrant nanostructures. (**a**) Two-step anodization, (**b**) through-hole AAO membrane fixed on a Si substrate as an evaporation mask, (**c**) depositing of the Cr nanoparticle array on the Si substrate, (**d**) selective XeF_2 isotropic etching of Si substrate using Cr nanoparticles as a mask, (**e**) removing Cr nanoparticles.

of Si (up to 66 GPa) is employed to obtain T-shaped reentrant nanostructure. Subsequently, an array of Cr nanoparticles with a thickness of approximately 50 nm was deposited onto the Si surface via AAO pores using electron beam evaporation (Fig. 5c). Then, the AAO membranes were removed with a commercial tape. The resulting Cr nanoparticle array on the Si substrates would serve as the subsequent etching template. The selective XeF_2 isotropic etching was employed to obtain T-shaped reentrant nanostructure on the Si substrate (Fig. 5d). Finally, a T-shaped reentrant nanostructure was formed after removing Cr nanoparticles from the Si surface (Fig. 5e). Despite its reentrant structure, the surface must still undergo chemical modification for increased resistance to wetting, then samples were treated with 1H, 1H, 2H, 2H-perfluoro-octyltrichlorosilane (PFOTS, Sigma–Aldrich) in the vapor phase at 140 °C for 5 min[25].

Theoretical modeling and simulation

A theoretical modeling of the wetting process, based on Marmur's[26] and Tuteja's works[25], was used to calculate the change in the Gibbs free energy density with the evolution of the solid–liquid interface for evaluating the stability of a composite interface on the T-shaped reentrant surface. Based on geometric parameters in Fig. 6a and the coordinate system in Fig. 6b, the formulations of geometric parameters are built as shown in Table 3.

Based on the theoretical modeling, a Matlab® (Mathworks Inc.) code was developed, and the areal Gibbs free energy density (G*) variation of the liquid drop was computed for water (γ_{lv} = 72.6 mN/m, θ = 120°) and hexadecane (γ_{lv} = 27.5 mN/m, θ = 80°). Herein γ is the surface tension, and subscripts s, v, and l represent solid, vapor and liquid, respectively.

From the thermodynamic perspective, the areal Gibbs free energy density of a given volume of liquid droplet at equilibrium on a substrate is given by the following equation

$$G^* = (2 - 3\cos\theta_{app} + \cos^3\theta_{app})^{-2/3}\left[2 - 2\cos\theta_{app} - \sin^2\theta_{app}(r_f f_s\cos\theta_{\text{int}} + f_s - 1)\right]. \quad (1)$$

Sample characterization

The fabricated Cr nanoparticles, unremoved AAO mask and T-shaped reentrant nanostructures were observed and their images were taken using field emission scanning electron microscopy (FESEM, FEI Nova NanoSEM 450). The liquid-repellent properties of liquid droplets on the sample surfaces were characterized using an optical contact-angle system (OCA20, Dataphysics, Germany). DI water of ~ 5 µL and hexadecane (Sigma-Aldrich) drops of ~ 2 µL were used as CA test solvents. To accurately express the wettability of the surface, the contact angle with 3–5 different positions on the surface was measured.

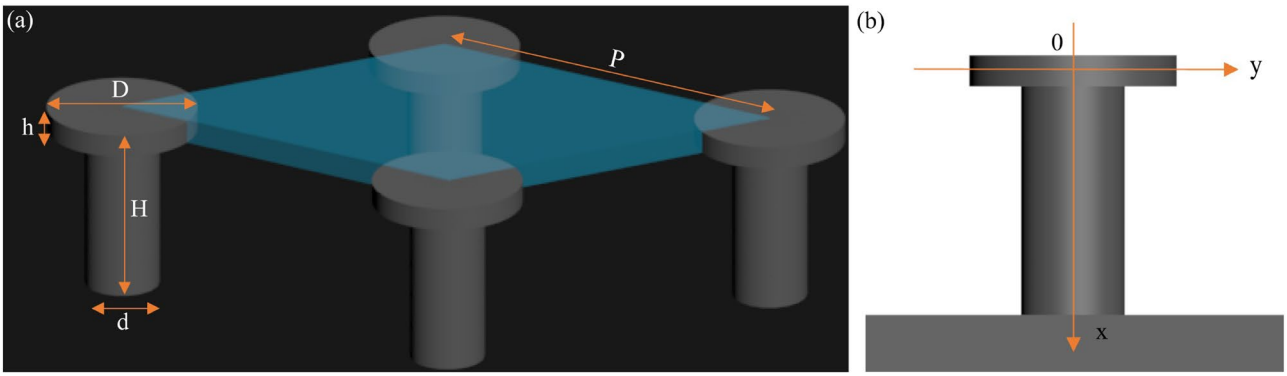

Figure 6. A schematic illustration of the topological profile in the calculation of the change in the Gibbs free energy density on the propagation of the liquid–air interface. (**a**) Geometric parameters in a discrete unit (blue area) with hexagonal arrangement, (**b**) the coordinate system used in the calculation. Herein D represents the diameter of T-shaped cap, d represents the diameter of T-shaped pillar, H represents the height of T-shaped reentrant nanostructures, h represents the height of T-shaped cap, P represents the pattern pitch of T-shaped reentrant nanostructures.

Parameters	0 ≤ x ≤ h	h < x < H	x = H
r_f	$1 + 4x/D$	$2D^2/d^2 + 4Dh/d^2 + 4x/d1$	$[\sqrt{3}/2(Pd)^2 + \pi D^2/2 + \pi d^2/4 + \pi Dh + \pi d(H-h)]/(\sqrt{3}/2P^2)$
f_s	$\pi D^2/(2\sqrt{3}P^2)$	$\pi d^2/(2\sqrt{3}P^2)$	1

Table 3. Formulations of geometric parameters for the hexagonal arrangement. Herein r_f is the roughness of wetted solid, defined as the actual wetted surface area divided by its projected surface area, f_s is the solid fraction, defined as the projected wetted surface area divided by the nominal surface area, θ_{int} is the intrinsic contact angle on the smooth and flat surface, θ_{app} is the apparent contact angle, G* is the areal Gibbs free energy density as a function of θ_{app} and x/H.

Data availability

The data used to support the findings of this study are available from the corresponding author upon request.

Received: 22 September 2023; Accepted: 8 December 2023
Published online: 11 December 2023

References

1. Zhang, M., Wang, P., Sun, H. & Wang, Z. Superhydrophobic surface with hierarchical architecture and bimetallic composition for enhanced antibacterial activity. *ACS Appl. Mater. Interfaces* **6**(24), 22108 (2014).
2. Zhang, X., Wang, L. & Levänen, E. Superhydrophobic surfaces for the reduction of bacterial adhesion. *RSC Adv.* **3**(30), 12003 (2013).
3. Tie, L., Li, J. & Liu, W. M. Customizing multiple superlyophobic surfaces in water-oil-air systems: From controllable preparation to smart switching via manipulating heterogeneous surface chemistry. *Appl. Surf. Sci.* **607**, 155028 (2023).
4. Tie, L. & Liu, W. M. Amphiphilic graphene oxide membranes for oil–water separation. *Sci. Bull.* **68**(4), 373–375 (2023).
5. Neinhuis, C. & Barthlott, W. Characterization and distribution of water-repellent, self-cleaning plant surfaces. *Ann. Bot.* **79**, 667–677 (1997).
6. Hemnath, A. & Sebastiraj, E. B. An overview of effect of lotus effect on the automotive windshield using titanium oxide. *Sci. Rev. Lett.* **2**(6), 487–490 (2014).
7. Varshney, P., Lomga, J., Gupta, P. K., Mohapatra, S. S. & Kumar, A. Durable and regenerable superhydrophobic coatings for aluminium surfaces with excellent self-cleaning and anti-fogging properties. *Tribol. Int.* **119**, 38 (2018).
8. Shang, Q. & Zhou, Y. Fabrication of transparent superhydrophobic porous silica coating for self-cleaning and anti-fogging. *Ceram. Int.* **42**(7), 8706 (2016).
9. Lee, S.-H. *et al.* Tunable multimodal drop bouncing dynamics and anti-icing performance of a magnetically responsive hair array. *ACS Nano* **12**(11), 10693 (2018).
10. Gao, H. *et al.* Biomimetic metal surfaces inspired by lotus and reed leaves for manipulation of microdroplets or fluids. *Appl. Surf. Sci.* **519**, 146052 (2020).
11. Dai, H. *et al.* Controllable high-speed electrostatic manipulation of water droplets on a superhydrophobic surface. *Adv. Mater.* **31**(43), 1905449 (2019).
12. Lai, X., Pu, Z., Yu, H. & Li, D. Inkjet pattern-guided liquid templates on superhydrophobic substrates for rapid prototyping of microfluidic devices. *ACS Appl. Mater. Interfaces* **12**(1), 1817 (2020).
13. Zhu, P. & Wang, L. Microfluidics-enabled soft manufacture of materials with tailorable wettability. *Chem. Rev.* **122**, 7010 (2022).
14. Vu, H. H., Nguyen, N.-T. & Kashaninejad, N. Reentrant microstructures for robust liquid repellent surfaces. *Adv. Mater. Technol.* **8**(5), 2201836 (2023).
15. Wang, N. & Xiong, D. Comparison of micro-/nano-hierarchical and nano-scale roughness of silica membranes in terms of wetting behavior and transparency. *Colloids Surf. Physicochem. Eng. Aspects* **446**, 8–14 (2014).
16. Leem, Y.-C. *et al.* Light-emitting diodes with hierarchical and multifunctional surface structures for high light extraction and an antifouling effect. *Small* **12**, 161 (2016).
17. Wu, T. Z. & Suzuki, Y. J. Design, microfabrication and evaluation of robust high-performance superlyophobic surfaces. *Sens. Actuators B Chem.* **156**(1), 401–409 (2011).
18. Melanie, M.-R. & Krasimir, V. Questions and answers on the wettability of nano-engineered surfaces. *Adv. Mater. Interfaces* **4**(16), 1700381 (2017).
19. Christo, S. N. *et al.* The role of surface nanotopography and chemistry on primary neutrophil and macrophage cellular responses. *Adv. Healthc. Mater.* **5**, 956 (2016).
20. Alhmoud, H. *et al.* Antibacterial properties of silver dendrite decorated silicon nanowires. *RSC Adv.* **6**, 65976 (2016).
21. Ostrikov, K., Macgregor-Ramiasa, M., Cavallaro, A., Ostrikov, K. K. & Vasilev, K. Bactericidal effects of plasma-modified surface chemistry of silicon nanograss. *J. Phys. D* **49**, 304001 (2016).
22. Prasad, K. *et al.* Synergic bactericidal effects of reduced graphene oxide and silver nanoparticles against gram-positive and gram-negative bacteria. *Sci. Rep.* **7**, 1591 (2017).
23. Lei, Y., Cai, W. & Wilde, G. Highly ordered nanostructures with tunable size, shape and properties: A new way to surface nano-patterning using ultra-thin alumina masks. *Prog. Mater. Sci.* **52**, 465–539 (2007).
24. Li, Z. P. *et al.* Fabrication of nanopore and nanoparticle arrays with high aspect ratio AAO masks. *Nanotechnology* **28**, 095301 (2017).
25. Tuteja, A., Choi, W., Mabry, J. M., McKinley, G. H. & Cohen, R. E. Robust omniphobic surfaces. *PNAS* **105**, 18200–18205 (2008).
26. Marmur, A. Wetting on hydrophobic rough surfaces: To be heterogeneous or not to be? *Langmuir* **19**(20), 8343–8348 (2003).

Acknowledgements

The authors acknowledge the support from Natural Science Foundation of Hubei Province of China (Grant Nos. 2021CFB418, 2022CFB369), National Scientific Research Project Cultivation program of Hubei University of Science and Technology (2023-25GP01).

Author contributions

Z.P.L. fabricated the samples; Q.W. and J.Q.W. carried out the experiments; Z.P.L. wrote the Original Draft while other authors provided review & editing; G.W. designed the research.

Competing interests

The authors declare no competing interests.

Additional information

Supplementary Information The online version contains supplementary material available at https://doi.org/10.1038/s41598-023-49445-y.

Correspondence and requests for materials should be addressed to G.W.